Alexandria Engineering Journal (2015) 54, 1057–1066

HOSTED BY

Alexandria University

Alexandria Engineering Journal

www.elsevier.com/locate/aej
www.sciencedirect.com

ORIGINAL ARTICLE

Image reconstruction technique using projection data from neutron tomography system

Waleed Abd el Bar [a,*], Imbaby I. Mahmoud [b], Hussein A. Konber [c], T. Mongy [a]

[a] Atomic Energy Authority (AEA), ETRR-2, P.O. Box 13975, Abu Zabal, Egypt
[b] Atomic Energy Authority (AEA), Research Centre, Engineering Department, Inshas, Cairo 11511, Egypt
[c] Al Azhar University, Electrical Engineering Department, Nasr City, Cairo 81624, Egypt

Received 23 October 2014; revised 29 March 2015; accepted 6 June 2015
Available online 26 June 2015

KEYWORDS

Image reconstruction;
Neutron tomography;
Filter back projection (FBP)

Abstract Neutron tomography is a very powerful technique for nondestructive evaluation of heavy industrial components as well as for soft hydrogenous materials enclosed in heavy metals which are usually difficult to image using X-rays. Due to the properties of the image acquisition system, the projection images are distorted by several artifacts, and these reduce the quality of the reconstruction. In order to eliminate these harmful effects the projection images should be corrected before reconstruction. This paper gives a description of a filter back projection (FBP) technique, which is used for reconstruction of projected data obtained from transmission measurements by neutron tomography system We demonstrated the use of spatial Discrete Fourier Transform (DFT) and the 2D Inverse DFT in the formulation of the method, and outlined the theory of reconstruction of a 2D neutron image from a sequence of 1D projections taken at different angles between 0 and π in MATLAB environment. Projections are generated by applying the Radon transform to the original image at different angles.

© 2015 Production and hosting by Elsevier B.V. on behalf of Faculty of Engineering, Alexandria University. This is an open access article under the CC BY-NC-ND license (http://creativecommons.org/licenses/by-nc-nd/4.0/).

1. Introduction

Neutron tomography (NT) is a powerful technique for three-dimensional visualization of hydrogenous substances such as rubber, water, oil, explosives, and wood even wrapped by thick metal layers. The experimental and safety conditions in different neutron sources such as nuclear reactors, spallation sources and standard particle accelerators make, in most cases, the facilities very different from each other. This implies that neutron tomography can yield information in cases where other NDT techniques fail. Neutron tomography already proved to be useful in many different areas such as archaeology, geology, biology, sciences, cultural heritages and industrial applications [1–3]. Fig. 1 shows the mass attenuation coefficients for thermal neutrons and 100 keV X-rays for the elements.

A neutron image is obtained by irradiating the object in an uniform neutron beam and recording the intensity transmitted by the object. Several solutions have been used for image recording: X-ray films and track-etch foils associated with converter screens (gadolinium, dysprosium and boron), neutron scintillators coupled to Charge Coupled Devices (CCD) video

* Corresponding author.
E-mail address: Engwaleed84@yahoo.com (W. Abd el Bar).
Peer review under responsibility of Faculty of Engineering, Alexandria University.

http://dx.doi.org/10.1016/j.aej.2015.06.003
1110-0168 © 2015 Production and hosting by Elsevier B.V. on behalf of Faculty of Engineering, Alexandria University.
This is an open access article under the CC BY-NC-ND license (http://creativecommons.org/licenses/by-nc-nd/4.0/).

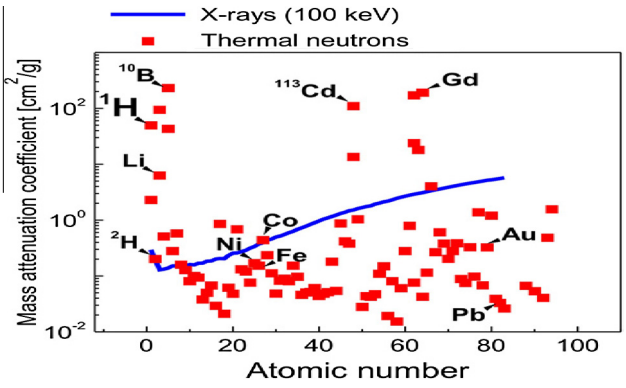

Figure 1 Mass attenuation coefficients for thermal neutrons and 100 keV X-rays for the elements (natural isotopical mixture unless stated differently) [2].

cameras and neutron imaging plates. The Neutron computed tomography can be used to obtain important 3-D information about the object's internal structure and material properties that other traditional methods cannot provide. Typically, a neutron computed tomography system consists of a neutron source with a collimator, a sample rotation device, a 2-D neutron imaging system and a motion control system which synchronizes sample rotation with the imaging system. A computer to capture, store and reconstruct the 3-D images is also needed. The first step in the development of a neutron tomography system is to select and optimize the neutron imaging and the second step is the preparation of the image data and subsequent calculation of the 3-D voxel array using one of many reconstruction techniques, such as a filtered back-projection or an algebraic reconstruction algorithm [4]. Tomography image visualization software that recombines the 2-D vertical images into a 3-D image is commercially available and is useful to analyze the 2-D image projections [5]. Fig. 2 shows the principle of computed tomography system.

ETRR-2 is an open pool type Material Testing Reactor (MTR) of 22 MW thermal power. The reactor is cooled and moderated by light water and reached first criticality in 1997. Irradiation facilities and beam tubes are installed at the reactor for research purposes as shown in Fig. 3. Neutron radiography facility is one of these beam tubes and was commissioned in 1999 using static based film neutron radiography [6].

The neutron radiography facility at ETRR-2 is upgrading from static based film (Nitrocellulose film and Agfa Structurix D7 photographic film) neutron radiography system into dynamic system neutron radiography/tomography by using Scintillation screens (ZnS (Ag)–6LiF) and a CCD-camera, and instrument was commissioned in January 2013.

2. Basic concepts

The image reconstruction techniques use the measured projection data as input to calculate the density distribution of the desired cross section of the investigated sample as output. Accordingly, the two dimensional image of the desired cross section can be obtained. The applicable reconstruction techniques are divided into three categories: first back-projection reconstruction, second by iterative reconstruction, and third by analytical reconstruction. The Filtered Back Projection (FBP) technique is used in most commercial medical scanners and has proved to be extremely accurate and amenable to fast implementation. This technique can be given a rather straightforward intuitive rationale because each projection represents a nearly independent measurement of the object. A brief discussion of the FBP is given below.

2.1. Projections

The Filtered Back Projection algorithm uses Fourier theory to arrive at a closed form solution to the problem of finding the linear attenuation coefficient at various points in the cross-section of an object. A fundamental result linking Fourier transforms to cross-sectional images of an object is the Fourier Slice Theorem [7–9].

Let x, y represent the coordinates inside the object (Fig. 4), and $f(x, y)$ the density (attenuation coefficient) in rectangular coordinates of the object under consideration at the cross-section at which the imaging has to be done. Let Eq. (2.1) represent the projection of the object at distance, t, from the center. The equation of the line AB is $= x\cos(\text{theta}) + y\sin(\text{theta})$, where we use "theta" (rotation angle) in place of the Greek symbol. Then, the projections are defined as [7]:

$$P_\theta(t) = \int_{(\theta,t)line} f(x,y)ds \tag{2.1}$$

It has been shown [3] that the above equation can be written using a delta function as:

$$P_\theta(t) = \int_{-\infty}^{\infty}\int_{-\infty}^{\infty} f(x,y)[\partial(x\cos(\theta) + y\sin(\theta) - t)dxdy] \tag{2.2}$$

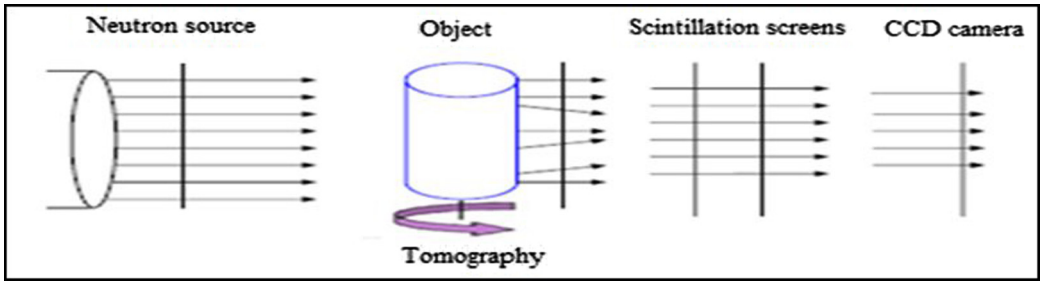

Figure 2 Principle of computed tomography.

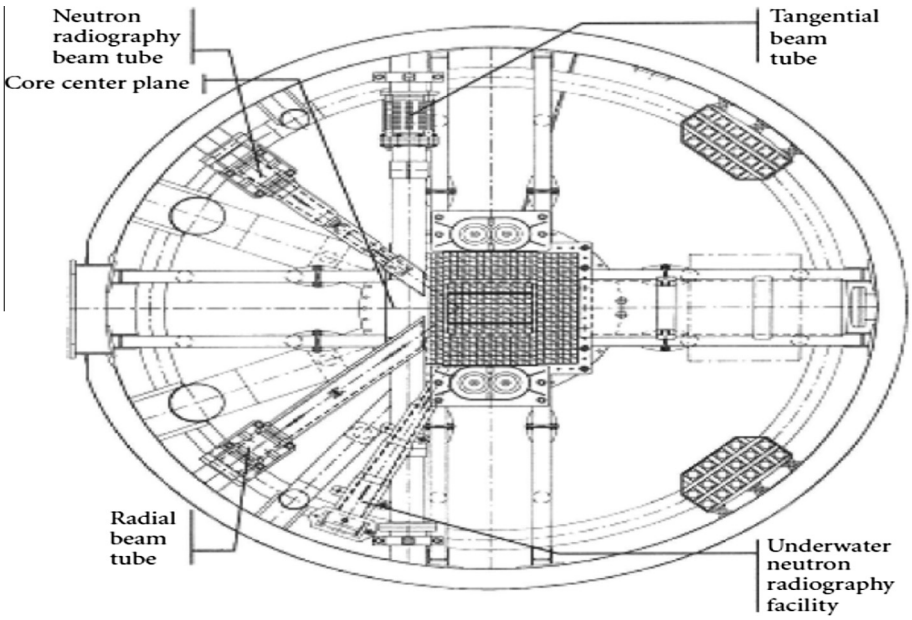

Figure 3 ETRR-2 beam tubes model [4].

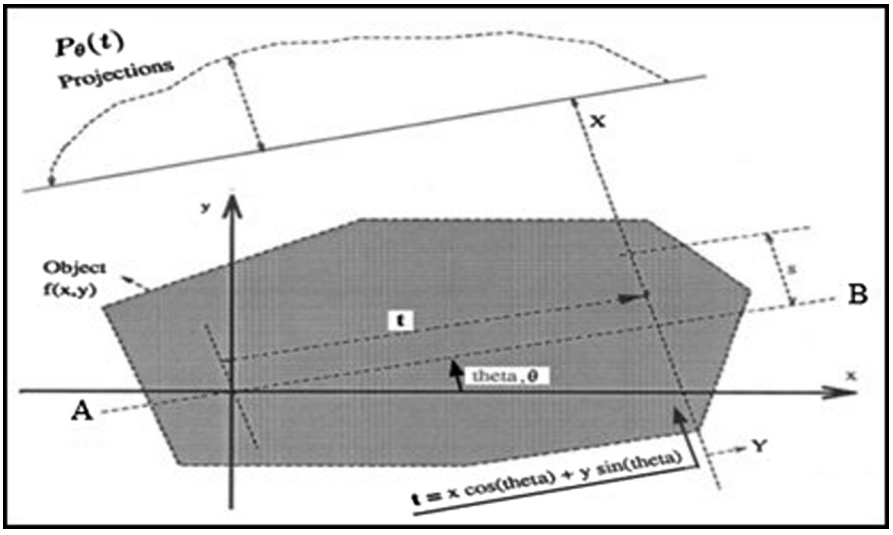

Figure 4 Formation of projections.

This function is known as the Radon transform of $f(x, y)$ [7]. A set of these functions for constant angle are the projections of the object at the cross-section where the rays are being passed. When the angle "theta" is held constant throughout a projection, we get parallel projection data.

2.2. Fourier Slice Theorem

An important result linking Fourier theory to the projections was developed by Bracewell and Riddle [10], Ramachandran and Lakshminarayanan [9,11]. The following proof is a result of Kak and Slaney [7]. The 2D Fourier transform is defined as:

$$F(u,v) = \int_{-\infty}^{\infty}\int_{-\infty}^{\infty} f(x,y)e^{-j2\pi(ux+vy)}dxdy \tag{2.3}$$

where u, v are measured in cycles/unit length. From the definition of the 1D Fourier transform, we can find the Fourier Transform of the projection data at any angle as:

$$S_\theta(\omega) = \int_{-\infty}^{\infty} p_\theta(t)e^{-j2\pi\omega t}dt \tag{2.4}$$

where ω is the in radians/unit length, we define a new coordinate system (t, s) defined by the rotation of the (x, y) system by the angle of rotation such that

$$\begin{bmatrix} t \\ s \end{bmatrix} = \begin{bmatrix} \cos\theta & \sin\theta \\ -\sin\theta & \cos\theta \end{bmatrix} = \begin{bmatrix} x \\ y \end{bmatrix} \tag{2.5}$$

In the (t, s) coordinate system, a projection would then be defined as

$$p_\theta(t) = \int_{-\infty}^{\infty} f(t,s)ds \tag{2.6}$$

From Eqs. (2.4) and (2.5)

$$S_\theta(\omega) = \int_{-\infty}^{\infty}\left[\int_{-\infty}^{\infty} f(t,s)ds e^{-j2\pi\omega t}\right]dt \tag{2.7}$$

$$S_\theta(\omega) = \int_{-\infty}^{\infty}\int_{-\infty}^{\infty} f(x,y)e^{-j2\pi\omega t}dxdy \tag{2.8}$$

$$t = x\cos(\theta) + y\sin(\theta) \tag{2.9}$$

The right hand sides of Eq. (2.8) represents the two-dimensional Fourier transform of the density $f(x, y)$ and the left hand side is the 1D Fourier transform of the projections. Therefore, taking the 1D Fourier transform of the projections of an object at an angle "theta" is equivalent to obtaining the two dimensional Fourier transform of the density $f(x, y)$ along the line "t" inclined at an angle "theta" Therefore if we take these projections at many angles, then we can get this 2D Fourier transform of the projections at many such lines inclined at various angles. If the number of angles is large enough, we will get many lines of 2D Fourier transforms of the object. If we now find the inverse Fourier transform of all these lines, we get the object's densities $f(x, y)$ for all (x, y) in the object's cross-section. That is,

$$f(x,y) = \int_{-\infty}^{\infty}\int_{-\infty}^{\infty} S_\theta(\omega)e^{j2\pi(ux+vy)}dudv \tag{2.10}$$

where

$$S_\theta(\omega) = F(\omega\cos\theta, \omega\sin\theta) = F(u,v) \tag{2.11}$$

2.3. The filtered back projection algorithm

Proof of the filtered back projection algorithm follows from Eq. (2.10) [7–9,11]. The following proof is due to Kak and Slaney [7]. If the coordinate system in the frequency domain (u, v) which is rectangular is changed to the polar coordinate system, we have to make the following substitutions:

$$u = \omega\cos\theta, \quad v = \omega\sin\theta, \quad dudv = \omega d\omega d\theta \tag{2.12}$$

$$f(x,y) = \int_0^{2\pi}\int_0^{\infty} F(\omega,\theta)e^{j2\pi\omega(x\cos\theta+y\sin\theta)}\omega d\omega d\theta \tag{2.13}$$

$$f(x,y) = \int_0^{\pi}\int_0^{\infty} F(\omega,\theta)e^{j2\pi\omega(x\cos\theta+y\sin\theta)}\omega d\omega d\theta + \int_\pi^{2\pi}\int_0^{\infty} F(\omega,\theta+\pi)e^{j2\pi\omega(x\cos(\theta+\pi)+y\sin(\theta+\pi))}\omega d\omega d\theta \tag{2.14}$$

From Fourier theory

$$F(\omega,\theta+\pi) = F(-\omega,\theta) \tag{2.15}$$

We get:

$$f(x,y) = \int_0^{\pi}\left[\int_{-\infty}^{\infty} F(\omega,\theta)|\omega|e^{j2\pi\omega(x\cos\theta+y\sin\theta)}d\omega\right]d\theta \tag{2.16}$$

From (2.4) and (2.7), we can say that in this case, $F(w$, "theta") inside the integral is the same as $S(w)$ of Eq. (2.7). Therefore,

$$f(x,y) = \int_0^{\pi}\left[\int_{-\infty}^{\infty} S_\theta(\omega)|\omega|e^{j2\pi\omega(x\cos\theta+y\sin\theta)}d\omega\right]d\theta \tag{2.17}$$

1. The filtered back projection algorithm can therefore be thought of as a three step process: Finding the Fourier Transform (FT) in 1D of the projections.
2. Finding the filtered projections. This essentially means multiplying the results of step 1. With a response function whose function looks as shown in Fig. 5. In the frequency domain, and then finding the inverse Fourier Transform (IFFT) (see Fig. 6).

$$Q_\theta(t) = \int_{-\infty}^{\infty} S_\theta(\omega)|\omega|e^{j2\pi\omega t}d\omega \tag{2.18}$$

$$FT^{-1}[Q_\theta(t)\cdot|\omega|] = \int_0^{\pi} Q_\theta(t) * h(x)d\theta \tag{2.19}$$

where $h(x) = FT^{-1}(|\omega|)$, representing the filter in spatial coordinates.

3. Finding the back projections. This step is the smearing of the filtered projections back on to the object, and is mathematically represented by

$$f(x,y) = \int_0^{\pi} Q_\theta(t)(x\cos\theta + y\sin\theta)d\theta \tag{2.20}$$

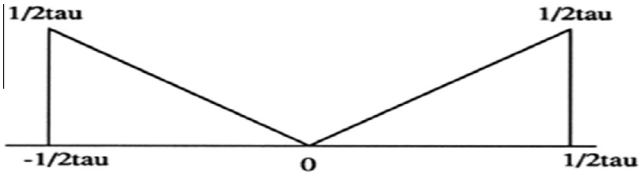

Figure 5 The response function in frequency domain.

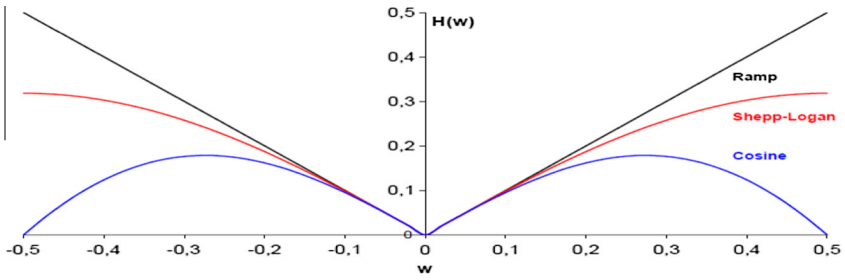

Figure 6 Filters in the frequency domain.

The inverse Fourier transform of $|\omega|$ does not exist because the integral does not converge. However, a solution can be found when considering the fact that in practice one has only a limited number of discrete samples. From the Nyquist theorem it follows that using a detector with pixel size Δ.

$$H(\omega) = |\omega| \cdot W(\omega) \tag{2.21}$$

in spatial coordinates.

$$h(x) = \int_{-1/2\Delta}^{1/2\Delta} |\omega| e^{j2\pi\omega x} d\omega \tag{2.22}$$

This represents the theoretically correct filter, but limited to the frequency band $[-1/2\Delta, 1/2\Delta]$. It is therefore known as the band limiting filter. The highest frequencies are amplified the most, and in practical circumstances these contain mostly noise. Therefore other filters have been described that attenuate these highest frequencies, leading to smoother and better looking reconstructions. Two well known filers are described below. The Shepp–Logan filter in frequency coordinates is given by:

$$H(\omega) = \left| \frac{1}{\pi\Delta} \sin(\pi\omega\Delta) \right| \cdot W(\omega) \tag{2.23}$$

The result in spatial coordinates is:

$$h(x) = \frac{2}{\pi^2\Delta(1-4x^2)} \tag{2.24}$$

This filter supposedly gives the best compromise between resolution and smoothness and is commonly used in medical imaging.

The Cosine filter in frequency coordinates is given by:

$$H(w) = |\omega| \cos(\pi\omega\Delta) \cdot W(\omega) \tag{2.25}$$

The result in spatial coordinates is:

$$h(x) = \frac{2}{\pi^2\Delta^2} \left(sign(x) \frac{\pi}{2} - \frac{1+4x^2}{1-4x^2} \right) \frac{1}{1-4x^2} \tag{2.26}$$

The cosine filter drastically reduces the high frequency content, resulting in smooth looking reconstructions.

3. Description of the setup for neutron tomography

The tomography setup was installed at the horizontal access of the thermal column of the RPI which is radial with respect to the reactor core. The main characteristics of the neutron beam at the irradiation position are shown in Table 1 [12].

Fig. 7 shows a schematic diagram of the installed setup for a typical tomography system the image is obtained by using a neutron Scintillation screens (ZnS (Ag)–6LiF) turntable object, a mirror, a cooled CCD camera and a computer support by using Labview. For every projection, the transmitted neutron intensity reaches the scintillator screen and the generated light is reflected by the mirror and recorded by the cooled CCD camera. Mirror bends the light path 90°. To take the necessary number of projections, the object is generally turned with a constant step from 0° to 180° or 360° [13]. In order to minimize radiation damages in the CCD caused by neutrons and gammas, the camera captures the light from the scintillator through a 45° mirror.

Fig. 7 shows the detection system in the neutron tomography facility. The camera and electronic components were shielded to protect them against neutrons and gamma. Boron carbide sheet were used to protect camera against neutrons. In the near future heavy concrete bricks will be

Table 1 Characteristics of the neutron beam at ETRR-2.

Rate intensity at beam outlet	3.3 Sv/h at 13.3 MW thermal
Thermal neutron flux at nominal power (22 MW)	1.5×10^7 n/cm^2 s
Fast neutron flux is at nominal power (22 MW)	1.6×10^6 n/cm^2 s
n/γ ratio	0.132×10^6 n cm^{-2} mR^{-1}
Cd ratio	10
L/D ratio	117
Facility resolution	188 μm (Agfa Structurix D7)

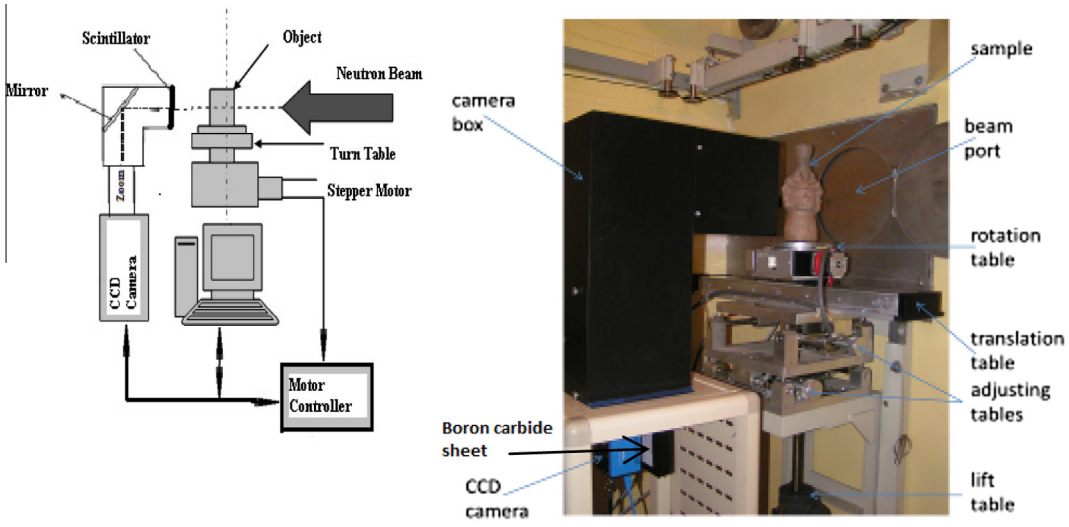

Figure 7 Detection system in the NR/T cell in ETRR-2.

placed in front of the camera to protect it against scattered gamma radiations.

4. Experimental details

Tomography experiment was performed at the imaging beam line at ETRR-2. Technical device (valve) was used as a sample with heterogeneous material composition – brass metal, plastic parts, sealing rings etc., Fig. 8.

For the tomographic measurement 200 projections at a rotation of 180° were used (0.9° per projection), take 10 open beam image without sample (Flat field) and 10 closed beam image (Dark field) with exposure time 30 s per image. The full data set was collected in 2 h. Dark current images or offset images were recorded with closed camera shutter and closed beam (see Figs. 9–15).

These images contain the electronic noise of the detector system caused by read out noise and dark current produced by the CCD-camera. Open beam images were taken without sample in the beam. For this purpose the controlling software translated the sample outside the beam by activating the linear stage. These images contain the inhomogeneities of the

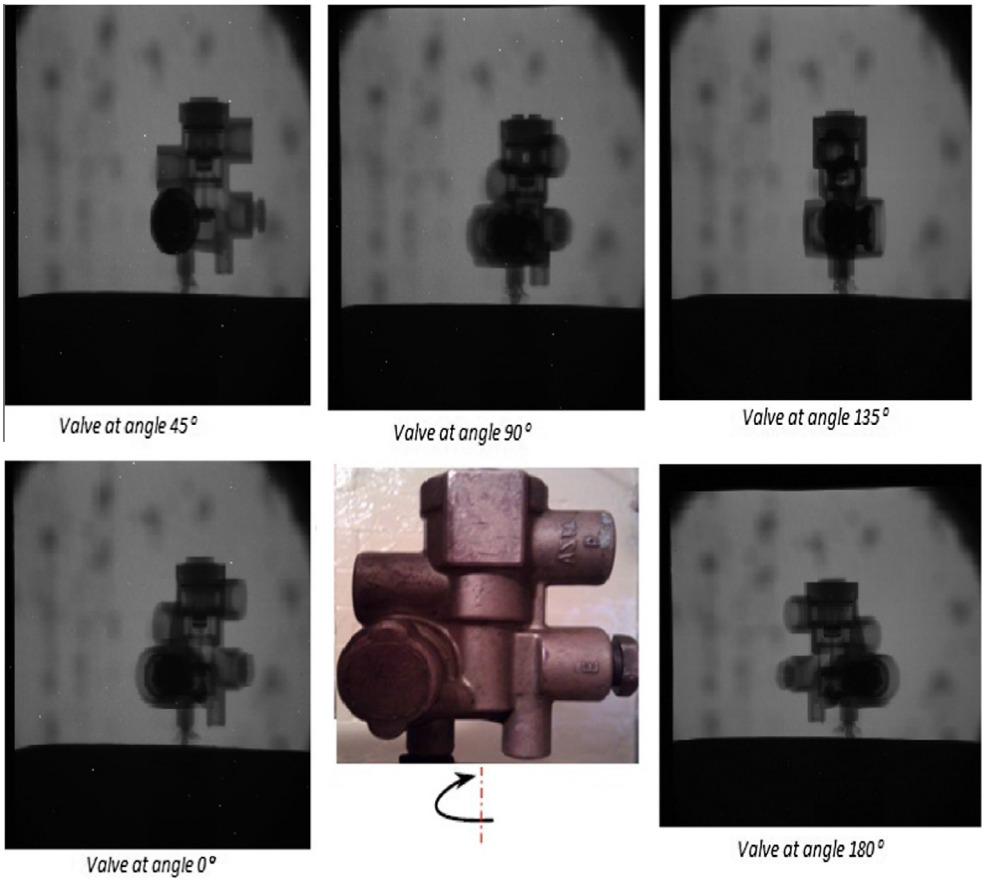

Figure 8 Neutron tomography of valve at different angle.

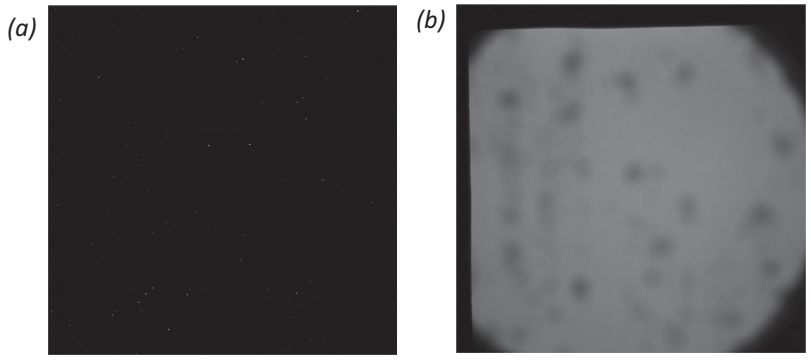

Figure 9 (a) Closed beam image (dark field) and (b) open beam image (flat field).

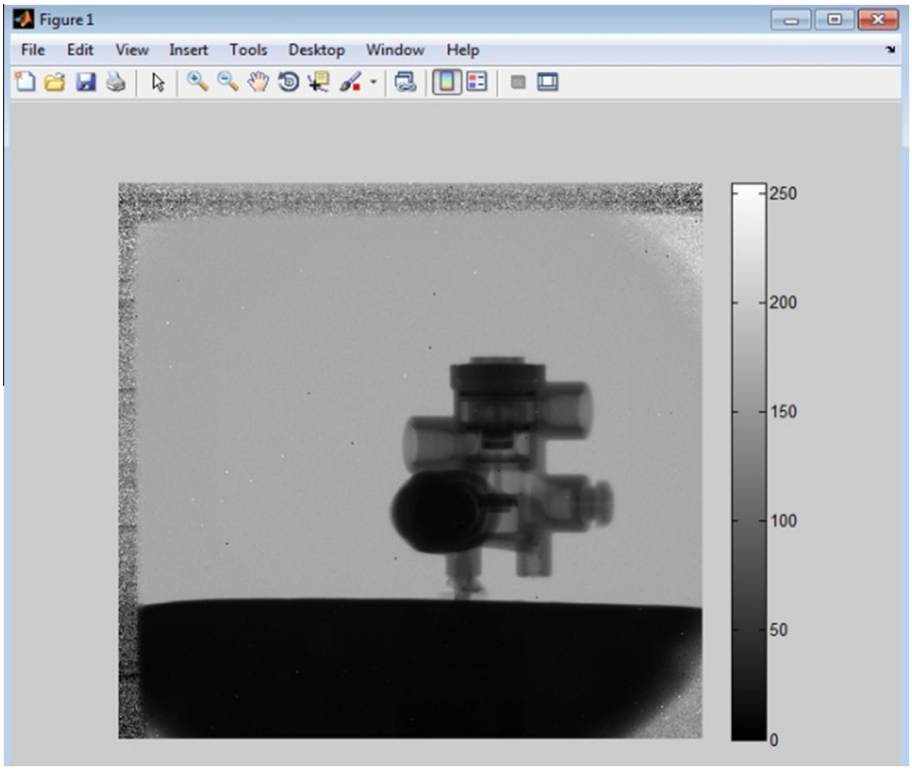

Figure 10 Neutron tomography of valve at angle 20° after normalizing.

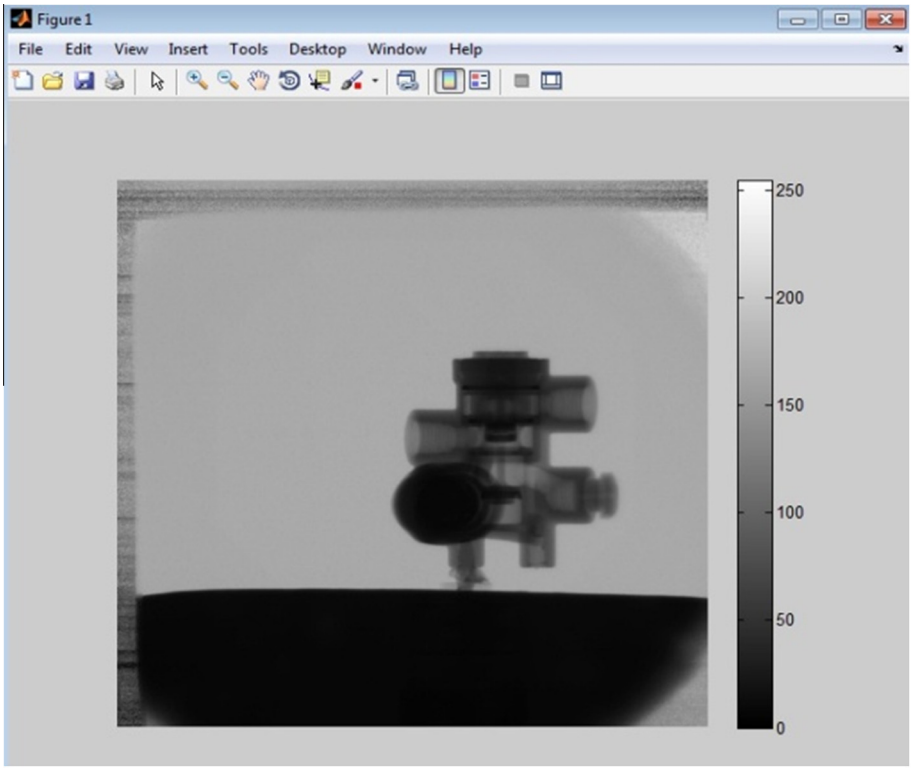

Figure 11 Neutron tomography of valve at angle 20° after median filter (3×3).

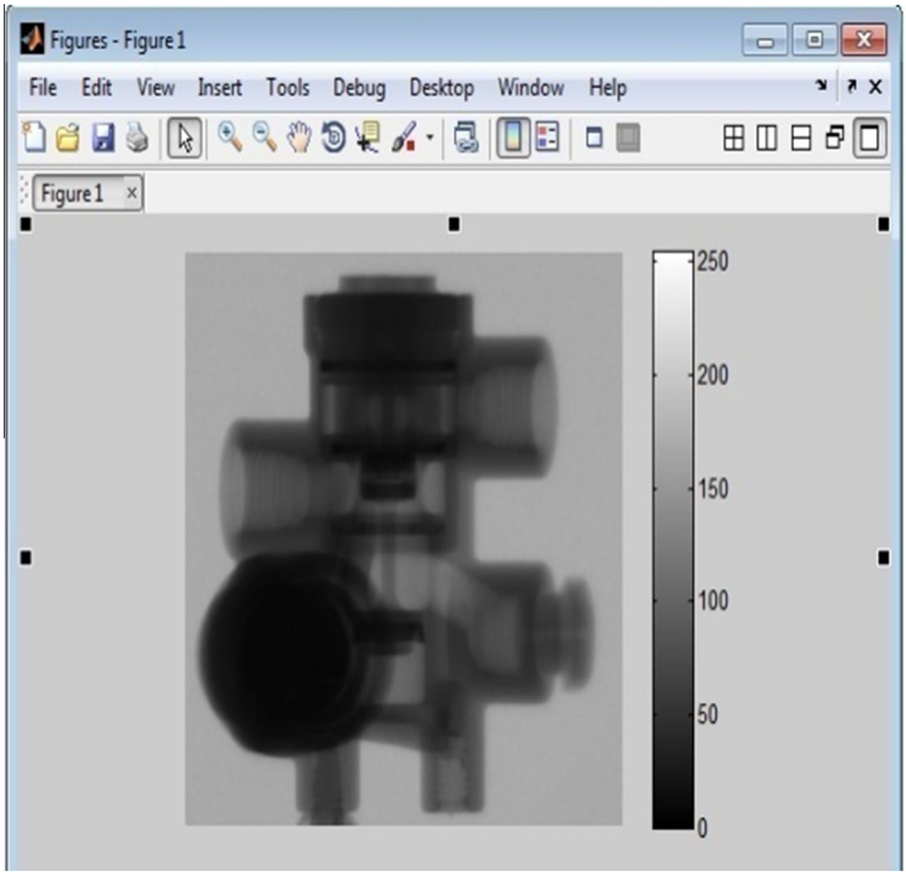

Figure 12 Neutron tomography of valve at angle 20° after cropping.

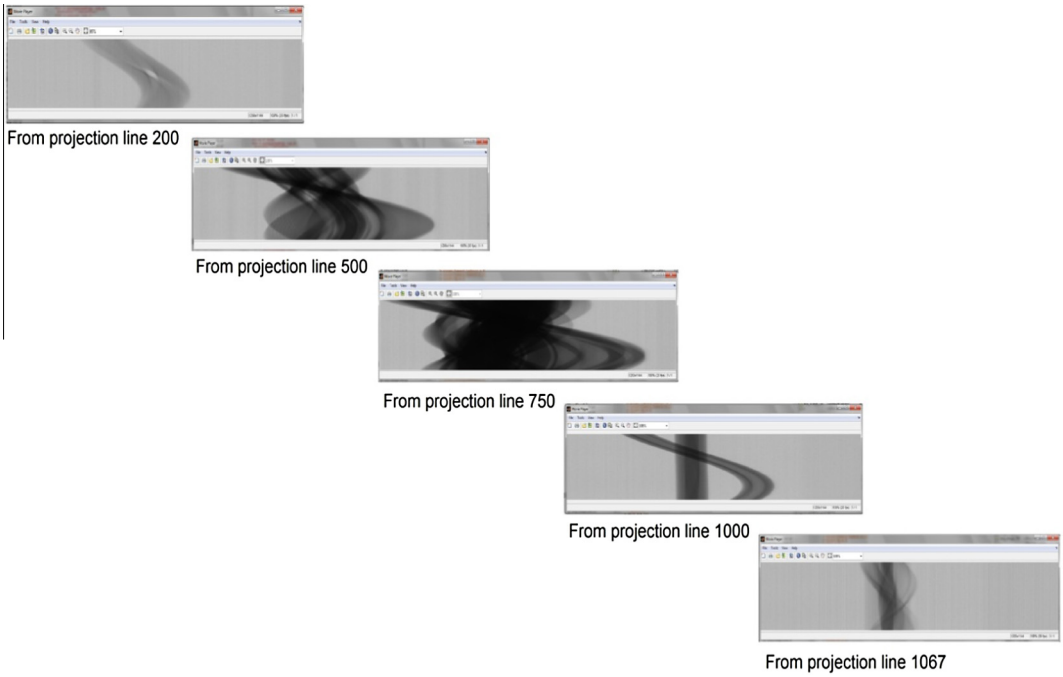

Figure 13 Sinogram image.

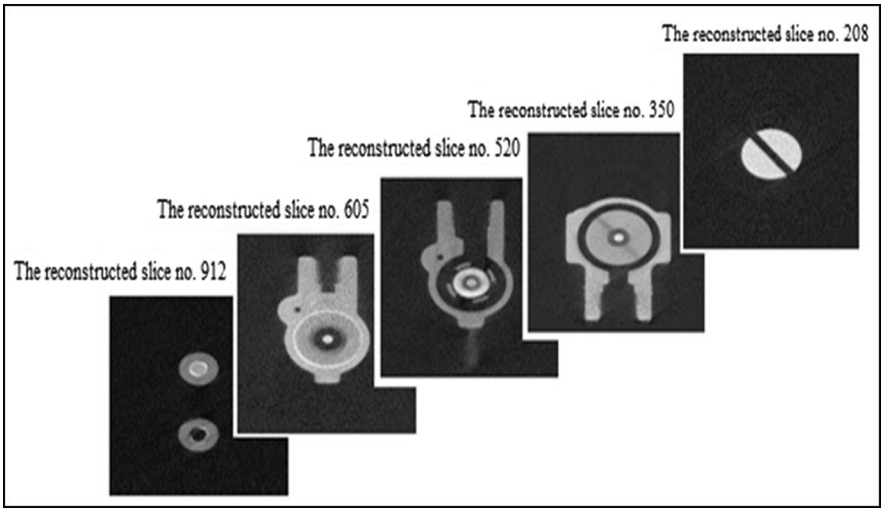

Figure 14 Neutron tomography slices.

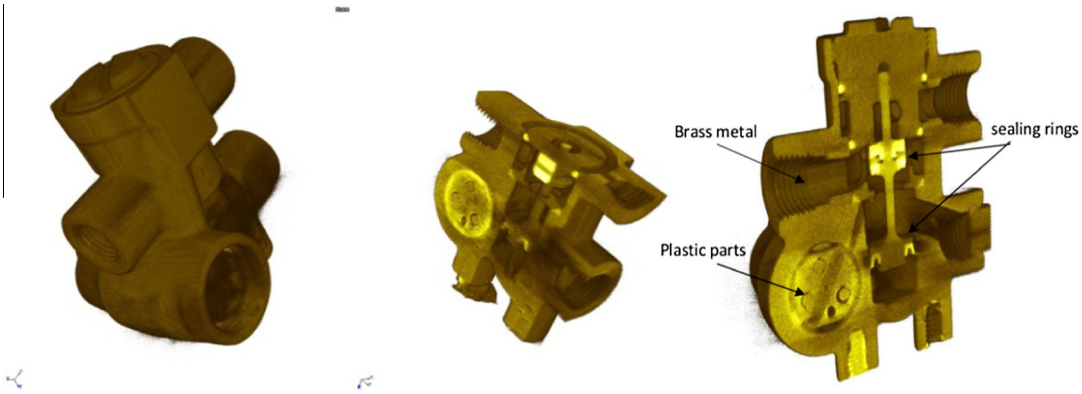

Figure 15 Tomographic reconstruction of the investigated sample.

neutron beam profile and the response of the detector system to the beam. Once the acquisition process of the Computerized Tomography (CT) scan is completed, the software lab (a part of the neutron imaging facility in ETRR-2) was used for data processing of the performed experiments providing successful tomographic reconstructions, 3D visualization and data analysis. The software lab was equipped with computer and software tools such as ImageJ, Matlab, Octopus and VGStudioMax as shown in Table 2.

The preparing of data for the reconstruction step by step is as in the following [14]:

Table 2 PC specification.

Data processing PC	FF825AV HP Z800 Workstation 1st Processor: Intel Xeon E5506 2.13 4 MB/800 QC 2nd Processor: Intel Xeon E5506 2.13 4 MB/800 QC Memory: 32 GB (8 × 4 GB) DDR3-1333 ECC HDD: 4 × 1000 GB SATA 7200
Control Pc	AU245AV HP Elite 8000 CMT Processor: Intel Core 2 Duo E7500 Memory: 2 GB PC3-10600 Memory (1 × 2 GB) HDD: 2 × 1000 GB SATA 7200

1. Correction of dark image taken with the closed shutter.
2. Correction of flat field.

$$\text{Normalized image}(x,y) = \frac{\text{tomography image}(x,y) - \overline{\text{dark current image}(x,y)}}{\overline{\text{open beam image}(x,y)} - \overline{\text{dark current image}(x,y)}} \tag{2.27}$$

3. Correction of white spot from every projection.
4. Selection of the area of interest, if it is needed.
5. Search of rotation axis.
6. Calculation of the attenuation coefficients.
7. Creation of sinogram.
8. Calculation of the 3-dimensional.
9. Visualization in Volume-Graphics software.

The quality of the tomographic investigation is sufficient to observe very fine details of the sample structure.

5. Conclusions

Neutron transmission tomography is an established nondestructive analysis method available at several neutron

radiography facilities around the world. It provides valuable complementary information to X-ray CT or other tomography modalities. The white-spots correction, dark field correction and flat field correction have been corrected by designed code in MATLAB another MATLAB code has been written, which enables convenient data preparation for the 3D reconstruction of sampled from 2D neutron transmission images taken from different view angles and got good result for 3D reconstruction image.

References

[1] M. Dierick, Tomographic Imaging Techniques using Cold and Thermal Neutron Beams, PhD Thesis Ghent University, 2005.

[2] M.A. Stanojev Pereira, R. Schoueri, C. Domienikan, F. de Toledo, The neutron tomography facility of IPEN-CNEN/SP and its potential to investigate ceramic objects from the Brazilian cultural heritage, Appl. Radiat. Isot. 75 (2013) 6–10.

[3] J. Banhart, Advanced Tomographic Methods in Materials Research and Engineering, University of Oxford Press, 2008.

[4] G.T. Herman, The Fundamentals of Computerized Tomography, Academic Press, New York, 1980.

[5] L. Shi, A.K. Heller, J. Brenizer, M.M. Mench, The Penn State University neutron computed tomography facility, in: Proceedings of the 8th World Conference Neutron Radiography, NIST, USA, 2006.

[6] M.A. Abou Mandour, R.M. Megahid, M.H. Hassan, T.M. Abd El Salam, Characterization and application of the thermal neutron radiography beam in the Egyptian Second Experimental and Training Research Reactor (ETRR-2), Sci. Technol. Nucl. Installations 2007 (2007). Article ID 24180, 6 pages.

[7] A.C. Kak, M. Slaney, Principles of Computerized Tomographic Imaging, IEEE Inc., IEEE Press, New York, 1988.

[8] H.H. Barrett, W. Swindell, Radiological Imaging: The Theory of Image Formation, Detection and Processing, Academic Press, New York, 1981.

[9] G.N. Ramachandran, A.V. Lakshminarayanan, Three dimensional reconstructions from radiographs and electron micrographs: application of convolution instead of Fourier transforms, Proc. Natl. Acad. Sci. 68 (1971) 2236–2240.

[10] R.H. Bracewell, A.C. Riddle, Inversion of fan beam scans in radio astronomy, Astrophys. J. 150 (1967) 427–434.

[11] A.V. Lakshminarayanan, Reconstruction from Divergent Ray Data, tech. rep., Dept. Computer Science, State University of New York at Buffalo, 1975.

[12] F. Esposto, Characterization of the neutron beam facilities, 0767-1330-3TABL-702-1O.

[13] <http://www.pco.de/categories/sensitive-cameras/pco2000/>.

[14] Wade J. Richard, Neutron Tomography Developments and Applications, UCD McClellan Nuclear Radiation Center, University of California Davis, 2003.